



OPEN

SUBJECT AREAS:

NANOSCALE
BIOPHYSICS

STRUCTURAL PROPERTIES

BIOINSPIRED MATERIALS

POLYMERS

Received
8 July 2013Accepted
11 October 2013Published
28 October 2013Correspondence and
requests for materials
should be addressed to
J.P.R. (jperez@mater.
upm.es)Identification and dynamics of
polyglycine II nanocrystals in *Argiope*
trifasciata flagelliform silkG. B. Perea^{1,2}, C. Riekel³, G. V. Guinea^{1,2}, R. Madurga^{1,2}, R. Daza^{1,2}, M. Burghammer³, C. Hayashi⁴,
M. Elices^{1,2}, G. R. Plaza^{1,2} & J. Pérez-Rigueiro^{1,2}¹Centro de Tecnología Biomédica. Universidad Politécnica de Madrid. 28223 Pozuelo de Alarcón (Madrid). Spain, ²Departamento de Ciencia de Materiales. ETSI Caminos, Canales y Puertos. Universidad Politécnica de Madrid. 28040. Madrid. Spain, ³European Synchrotron Radiation Facility. B.P. 220, F-38043, Grenoble Cedex, France, ⁴Department of Biology. University of California, Riverside. CA 92521. USA.

Spider silks combine a significant number of desirable characteristics in one material, including large tensile strength and strain at breaking, biocompatibility, and the possibility of tailoring their properties. Major ampullate gland silk (MAS) is the most studied silk and their properties are explained by a double lattice of hydrogen bonds and elastomeric protein chains linked to polyalanine β -nanocrystals. However, many basic details regarding the relationship between composition, microstructure and properties in silks are still lacking. Here we show that this relationship can be traced in flagelliform silk (Flag) spun by *Argiope trifasciata* spiders after identifying a phase consisting of polyglycine II nanocrystals. The presence of this phase is consistent with the dominant presence of the -GGX- and -GPG- motifs in its sequence. In contrast to the passive role assigned to polyalanine nanocrystals in MAS, polyglycine II nanocrystals can undergo growing/collapse processes that contribute to increase toughness and justify the ability of Flag to supercontract.

Flagelliform (Flag) silk and major ampullate gland silk (MAS) are the two most studied silks among those spun by spiders and, although their biological functions differ, were found to share the conserved motifs -GPG- and -GGX⁻¹. MAS is widely considered as the reference spider silk due not only to its unrivalled combination of tensile strength and strain at breaking², but also to the development of techniques that allow access to large amounts of material³. Its tensile properties are explained by a double lattice model⁴ consisting of a mesh of hydrogen bonds established between the protein residues, superimposed to a mesh of elastomeric protein chains⁵ anchored to protein nanocrystals⁶. This model accounts qualitatively for the most remarkable properties of spider silks, including the ability to supercontract⁷, and fits nicely to the protein sequence⁸. In this regard, it was found that one of the main motifs of sequence present in MAS spidroin, the polyalanine runs (-A_n-), pile up to form β -nanocrystals. The exact role of the other three conserved motifs -GA- and, especially, of those shared with Flag -GGX- and -GPG⁻¹ is much less clear.

Flagelliform (Flag) silk is the silk used by orb-web spiders in the core of the sticky viscid line that makes up the spiral of the web. Flag represents another rich opportunity to study the relationship between composition, microstructure and behaviour in silks, since it also shows remarkable tensile properties^{9,10} and the ability to supercontract¹¹, but its sequence differs significantly from that of MAS. In this regard, Flag silk is characterized by the complete absence of the polyalanine motif in its sequence, and by the extensive presence (over 90% of the total sequence) of the motifs -GGX-, -GPG- and a longer motif known as spacer. Despite an obvious interest in the detailed study of Flag silk, previous attempts were confounded by the presence of the aggregate silk coating¹². As described below, application of a combined methodology consisting of (1) removing the viscous coating, and (2) getting an accurate measurement of the cross sectional area allowed characterizing Flag silk spun by *Argiope trifasciata* spiders with unprecedented detail in terms of mechanical behavior and microstructure.

Results

Figure 1a shows the true stress-true strain curves of Flag fibers after removal of the viscous coating, and being subsequently subjected to wet stretching processes defined by different values of the alignment parameter, α ¹³. At least four samples were tested for each value of the alignment parameter and their main mechanical parameters

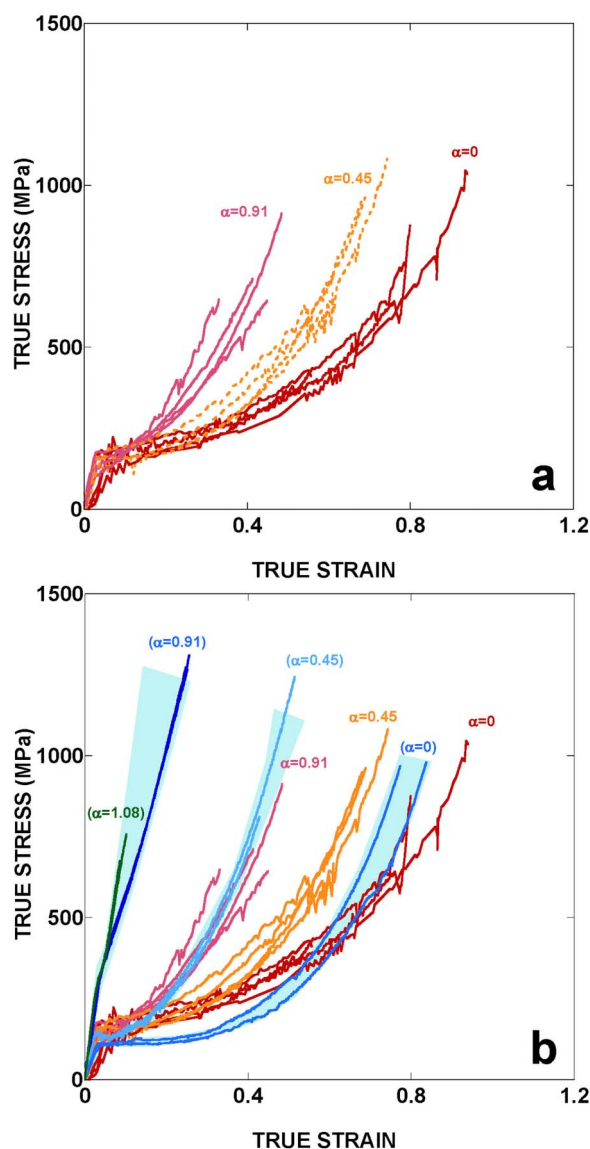


Figure 1 | Tensile properties of flagelliform fibers. (a) True stress-true strain curves of flagelliform fibers subjected to different wet stretching processes as defined by the alignment parameter, α . (b) Comparison of the tensile properties of flagelliform and MAS fibers, and its dependence on the parameter α . The range of properties exhibited by MAS fibers is shaded blue.

are presented in Table 1. The wet stretching process was initially developed for tailoring the tensile properties of MAS fibers and proceeds by stretching the fiber in water from the initial maximum supercontracted length, L_{MS} , to a selected length, L_C . Water is then removed and the fiber allowed to dry. The alignment parameter is defined as $\alpha = L_C/L_{MS} - 1$, so that a value of $\alpha = 0$ corresponds to maximum supercontracted fibers, and represents the *ground state* of the fiber. The existence of a ground state that is reached after maximum supercontraction allows extrapolating this process to Flag fibers.

As shown by the concurrence of the curves with the same value of α , and by the small scattering of the mechanical parameters (see Table 1), it is demonstrated that this procedure allows obtaining Flag fibers with reproducible and predictable mechanical properties, as previously found in MAS fibers¹³. The maximum value of α attainable for Flag silk is approximately $\alpha = 0.9$, since all trials for obtaining fibers with an alignment parameter significantly higher than this value failed due to the breaking of the fiber.

Table 1 | Mechanical properties of Flag fibers with different values of the alignment parameter, α

α	E_{initial} (GPa)	σ_u (GPa)	ϵ_u	W_F (J/m ³)
0 (MS)	5 ± 1	800 ± 100	0.76 ± 0.08	250 ± 50
0.45	7 ± 1	900 ± 100	0.67 ± 0.03	250 ± 20
0.9	6.5 ± 0.6	730 ± 70	0.41 ± 0.04	140 ± 20

E_{initial} : slope of the initial linear part of the true stress-true strain curve. σ_u : True stress at breaking. ϵ_u : True strain at breaking. W_F : Work to fracture, measured as the area under the stress-strain curve up to the breaking point. Values shown as mean value \pm standard error.

X-Ray diffraction patterns obtained from samples with values of the alignment parameter $\alpha = 0, 0.45$ and 0.91 are shown in Figure 2. The existence of a crystalline phase in Flag fibers, which was previously disputed based on other microstructural techniques that suggested a completely amorphous microstructure¹⁴, appears unequivocal from the XRD data. Although Raman microscopy has revealed a content of β -pleated sheets that represents approximately 10% of the total protein¹⁵, the analysis of the diffraction spots indicates that the patterns are not compatible with the unit cell of β -nanocrystals. In particular, their characteristic (020) reflection¹⁶ is absent from Flag patterns, and the (003) reflection found in Flag, which corresponds to the periodicity along the polypeptide backbone, differs from that of β -pleated sheets. The measured diffraction patterns are compatible with a tetragonal unit cell with parameters (mean value \pm standard error) $a = b = 0.455 \pm 0.002$ nm, $c = 0.922 \pm 0.002$ nm (chain direction). As indicated above, this unit cell does not correspond to the usual β -nanocrystalline microstructure¹⁷, but is consistent with the formation of nanocrystals built from polyglycine II helices (Figure 2b), as supported by the simulation of the diffraction pattern of this structure¹⁸ (Figure 2c). The presence of polyglycine II nanocrystals is also consistent with the sequence of Flag silk with a large content of glycine rich motifs, that can acquire a polyglycine II conformation¹⁹.

In addition, access to the diffraction patterns of fibers with different values of α allows determining their dynamics during stretching or, conversely, supercontraction. No change in the unit cell is observed with varying values of α . However, crystallinity, and the size and orientation of the nanocrystals appear to be strongly influenced by this value (Figure 3). In this regard, the nanocrystals are shown to align with the macroscopic axis of the fiber (Figure 3a), and crystallinity increases steadily with increasing values of α ($\chi = 5\%$ at $\alpha = 0$ and $\chi = 10\%$ at $\alpha = 0.9$) (Figure 3b), as previously described in MAS²⁰. In contrast to the constancy shown by the dimensions of MAS nanocrystallites with increasing α , the size of Flag nanocrystals is observed to vary and these variations are found to depend on the crystallographic direction. Thus, it is found that the length $L_{(100)}$ decreases with increasing α , meanwhile the length $L_{(003)}$ (approximately parallel to the macroscopic axis of the fiber) shows the opposite behavior (Figure 3c).

AFM analysis of maximally supercontracted Flag fibers ($\alpha = 0$) reveals a nanoglobular microstructure comparable to that found in other natural and artificial silk fibers²¹ (Figure 4). The nanoglobules were approximated by ellipses with sizes 11 ± 3 nm (major axis, with a maximum value of 20 nm) and 8 ± 2 nm (minor axis).

Discussion

Combination of the mechanical and microstructural data presented above allows establishing a coherent picture of the behaviour of Flag silk, in which the dynamics of polyglycine II nanocrystals are assigned a leading role. Thus, the overall true stress-true strain curves presented in Figure 1 are compatible with the assumption of three regimes in the mechanical behaviour of silks: initial deformation of hydrogen bonds, yielding of the protein chains from their initial configuration and stretching of the protein chains^{22,23}. In this context,

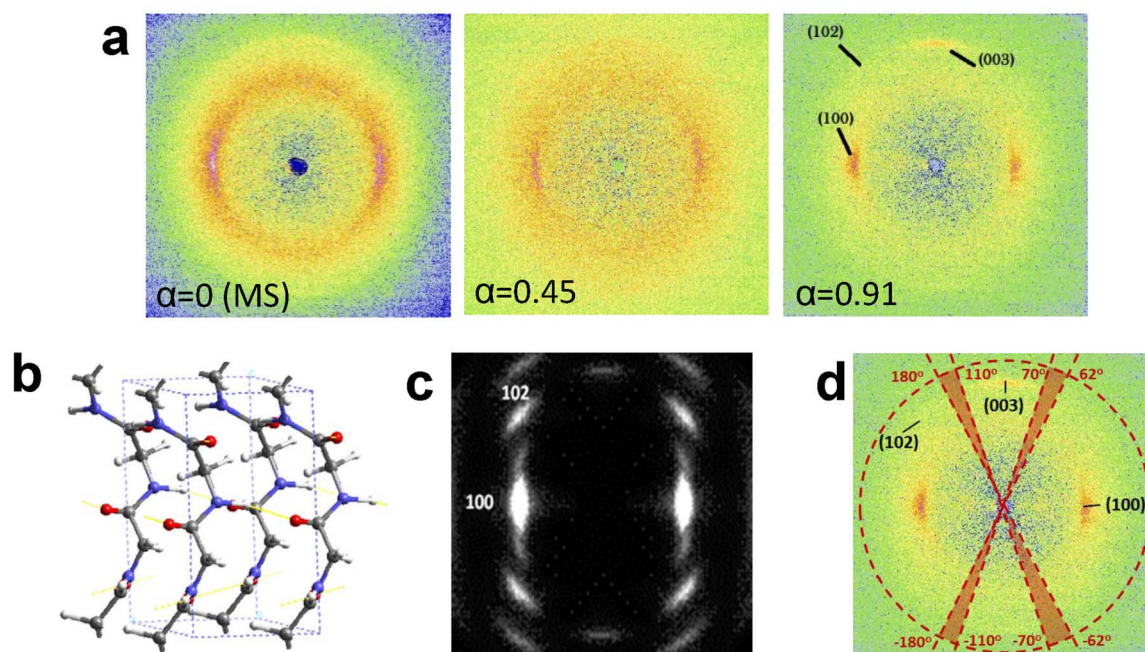


Figure 2 | X-Ray diffraction analysis of flagelliform fibers. (a) Diffraction patterns of flagelliform fibers with different values of α . (b) Proposed unit cell of the polyglycine II nanocrystals. (c) Simulated spectrum of a polyglycine II nanocrystal obtained with the Cerius program (Courtesy of C. Riekell). (d) Scheme of the areas selected to obtain the average intensity of the amorphous halo required for integration of the Bragg peaks in order to calculate crystallinity, χ .

the increase in polyglycine II crystallinity would be the result of conformational changes induced in the proteins during the stretching step.

Consistently with this model, it is found that crystallinity increases reversibly during the stretching of the fiber from the ground (i.e. maximum supercontracted) state due to the increase of the nanocrystal size along the direction parallel to the macroscopic axis of the fiber. This process can be reverted by supercontraction which, in turn, is shown to consist of the partial collapse of the nanocrystals. All these changes can be accounted for if it is assumed that stretching leads to a molecular reorganization of spatially close protein chains at the ends of polyglycine II nanocrystals. In this regard, fibers with larger values of α are shown to attain lower values of strain at breaking, since the conformational changes of the proteins are limited compared with those of fibers with lower values of α . With respect to its influence on the tensile behaviour, this mechanism of nanocrystal formation allows dissipating mechanical energy and, consequently, should represent a significant contribution to toughness.

The parallels and differences observed between Flag and MAS immediately suggest the question of whether these features might represent general design principles in spider silks. Although not direct evidence of the presence of polyglycine II nanocrystals in MAS is presented in this work, several indirect facts indicate that this might be the case.

Comparison of the tensile properties of Flag and MAS show a striking resemblance between the stress-strain curves of both materials at low values of α (Figure 1b). Significant differences are observed at increasing values of α , since the tensile strength of Flag silk does not increase with α , leading to an overall decrease in its work to fracture. Both silks also differ in the curvature of the stress-strain curves, which changes from convex to concave in MAS at large values of α , but remains convex in Flag independently of α , although this difference could be related with the larger values of α found in MAS, up to $\alpha = 1.44$.

The improved behavior of MAS at large values of α could be related with the presence of the β -nanocrystals¹⁶. Previous studies have shown that the crystalline unit cell and the size of the

β -nanocrystals does not change during either stretching²⁴ or supercontraction²⁵. However, the orientation of the nanocrystals with respect to the axis of the fiber and the crystalline fraction increase during stretching²⁴. Supporting the importance of β -nanocrystals for the tensile behaviour at large strains, it was found by simulation that the length of the polyaniline runs in the sequence are optimized for the formation of β -nanocrystals²⁶, whose size, in turn, is optimized to promote a redistribution of stresses in the material²⁷.

The combined effect of β - and (presumably) polyglycine II nanocrystals in MAS could explain the change from convex to concave curvature of the stress-strain curves at high values of α . Concave (convex) curvature of a stress-strain curve is usually labelled as *enthalpic* (*entropic*) behaviour and indicates that variations in the intensity of the interactions (conformational variations) are responsible for the performance of the material. The formation of polyglycine II nanocrystals in MAS would justify this transition since, after the extensive formation of the nanocrystals at large values of α , further stretching would imply the deformation of the nanocrystals, and not additional conformational changes in the chains.

Evidently, it is necessary to assess the question of whether the results found in Flag can be extrapolated to MAS. The presence of a second ordered phase in MAS that differed from the β -nanocrystals had been suggested previously^{28,29}, and its presence at the ends of the polyaniline nanocrystals have been established by different microstructural techniques^{30,31}. Most studies³² have extrapolated the β -pleated microstructure of the underlying polyaniline nanocrystals to the second ordered phase, but our present study suggests that the possibility of finding polyglycine II structures formed at the end of the β -nanocrystals should be considered. In addition, the XRD data presented in this work can justify the origin of the difficulty of identifying polyglycine II nanocrystals in MAS. Thus, it is found that the most intense reflection arising from polyglycine II nanocrystals corresponding to (100) overlaps with the much more intense reflections (020) and (210) arising from the polyaniline β -nanocrystals. There is, however, at least one report³³ on MAS silk in which a diffuse scattering ring with a Q close to that of the (210) reflection is observed, that is particularly strong along the polar direction.

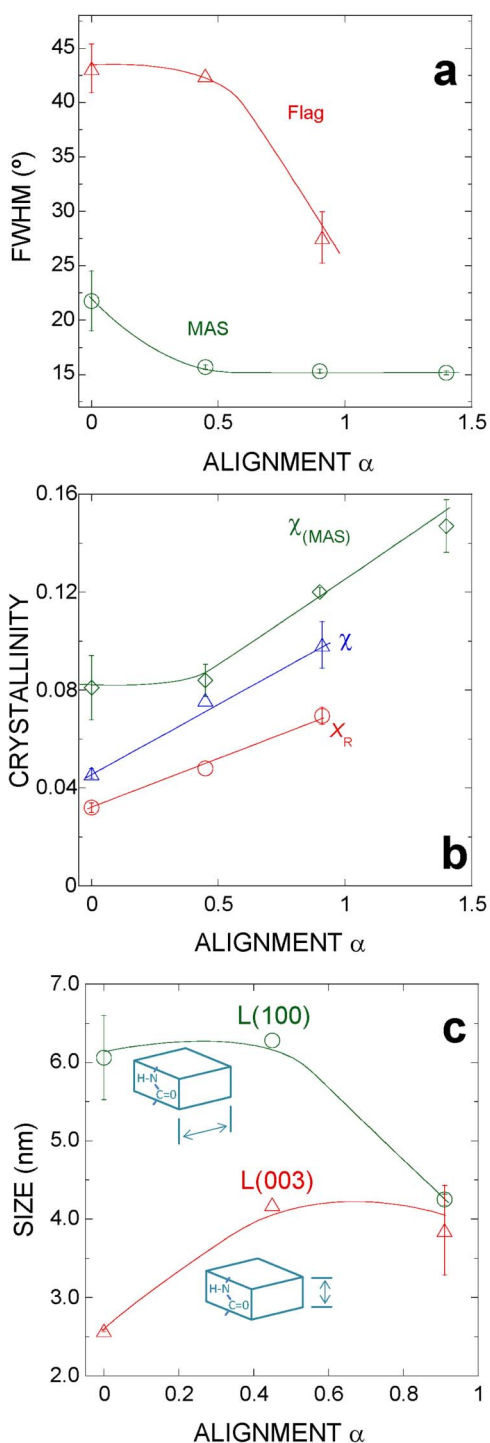


Figure 3 | Variation of the nanocrystal parameters with different values of α . (a) Orientation of the nanocrystals as measured from the FWHM of the gaussian used to fit the azimuthal profile of the equatorial Bragg peak (100). Corresponding values in MAS are included to facilitate comparison. Error bars represent standard error. (b) Variation of crystallinity as measured by (i) X_R , ratio between the intensity of the (100) peak and the total intensity of a nearby section, and (ii) χ , ratio between the intensity of Bragg peaks and total intensity²⁰. Data corresponding to MAS are shown for comparison. (c) Variation of the size of the nanocrystals in Flag along two perpendicular directions, (100) and (003), as calculated from the Scherrer's equation.

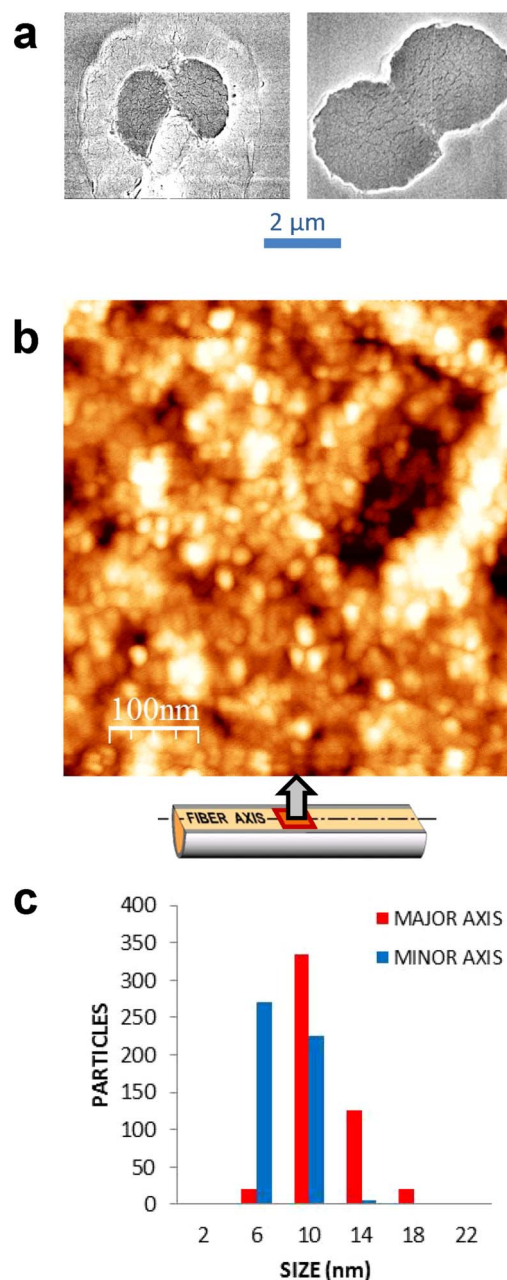


Figure 4 | SEM and AFM characterization of flagelliform silk. (a) Two representative SEM micrographs used for computing the cross-sectional area of flagelliform fibers. The two individual filaments (each filament known as a brin) that make up the fiber (bave) are clearly identified. (b) AFM image of a longitudinal section of a Flag fiber subjected to maximum supercontraction (MS, $\alpha = 0$). The macroscopic axis of the fiber lies along the horizontal direction. Nanoglobules are approximated by ellipses and the histogram shows the distribution of sizes along the major and minor axes.

Furthermore, there are three indirect experimental evidences that substantiate the presence of polyglycine II nanocrystals in both Flag and MAS. (1) Comparison of the Flag and MAS sequences shows that both silks share the polyglycine II nanocrystal-forming motifs. This fact is also consistent with the simultaneous evolutionary occurrence of supercontraction and the $-GGX-$ and $-GPG-$ motifs³⁴. In this regard, the analysis of recombinant Flag silk including the spacer region besides the glycine-rich motifs³⁵ suggests that the spacer might play a role in facilitating the alignment of the other two motifs.



However, the properties of recombinant Flag fibers are still below from those of the natural material, so that extrapolating conclusions from recombinant to natural Flag fibers should be taken cautiously. (2) When the increase of crystallinity with α is analysed (Figure 3b), it is found that both silks present the same slope of the crystallinity vs. α curves, except for the presence of an initial offset in MAS²⁰. This observation could be explained in part by the formation of the polyglycine II crystals in MAS, after completing the initial rotation of the polyalanine β -nanocrystals³⁶. (3) Finally, the size of the nanoglobules observed by AFM was correlated with the longest crystal-forming fragments in silkworm silk²¹ and minor ampullate gland silk³⁷. This correlation failed in MAS if the longest polyalanine fragments were considered, but combination of sequential polyalanine fragments ($-A_8-$ corresponds to 3.5 nm if β -pleated conformation is assumed) and various $-GGX-$ or $-GPG-$ (approx. 0.65 nm each if polyglycine II conformation is assumed) would yield values close to the experimental size of 10–14 nm.

Methods

Flagelliform fibers were obtained from webs built by *Argiope trifasciata* spiders and the coating (aggregate silk gland secretions) on the samples was eliminated by centrifugation¹¹. The supercontraction procedure of cleaned Flag fibers was based on that used on MAS fibers, with some modification. The slack, clean fiber was immersed in water at 20°C for at least 10 minutes and then allowed to dry overnight. However, it was found that the maximum supercontracted state was rarely reached in a single step. Consequently, the fiber was stretched in air up to a strain of 0.4 and allowed to supercontract again. The force-displacement curve obtained after the second supercontraction step was compared with that recorded after the initial supercontraction. If both curves did not concur, the fiber was subjected to approximately thirty loading and unloading cycles (strain amplitude ± 0.2 ; strain rate 0.2 min⁻¹) and subjected to an additional supercontraction step. This procedure was repeated until the force-displacement curves between two consecutive cycles concurred. The wet stretching process of maximum supercontracted Flag fibers proceeded as initially developed for MAS fibers¹³. A novel procedure was developed for measuring the cross sectional area of Flag fibers consisting of staining the fibers with Richardson methylene blue, embedding in Spurr resin and using ultramicrotomy.

Tensile tests¹³ were performed with a displacement speed of 1 mm/min at environmental conditions 20°C and 35% RH. True stress (σ) and true strain (ϵ) curves were calculated from the force-displacement curves and the cross sectional areas of the fibers (Figure 4a) assuming the constant volume hypothesis³⁸.

XRD images were obtained using synchrotron radiation at the ESRF-ID13 in Grenoble, (France) using a monochromatic beam from crossed mirrors of size $\approx 1 \times 1 \mu\text{m}^2$ and a wavelength of 0.1 nm, as explained in detail elsewhere²⁰. Two Flag samples were studied for each alignment parameter, α . A scan of 256 images was performed on each sample including patterns inside and outside the fiber. Patterns recorded outside the fiber were used for determining the background. Compared with diffraction patterns of other silks¹⁶, Flag patterns tend to be noisier due to the small average diameter of the fibers in the range 1–2 μm . Diffraction pattern analysis was performed with the FIT2D program³⁹. XRD data were used to study the unit cell of the fibers, their crystallinity, the sizes of the nanocrystals and their orientation with respect to the macroscopic axis of the fiber¹⁶.

The crystallinity of the samples was estimated with two alternative methods. In the first method a section of an image which includes the brightest peak (100) is selected and integrated azimuthally. The resulting radial profile can be fitted²⁰ with four Gaussians and a 0-order polynomial function. The sharpest Gaussian is customarily associated with the crystalline fraction contributing to the (100) peak. In the same sense, the broadest Gaussian is assigned to the amorphous fraction, and the two remaining Gaussians are supposed to represent weakly oriented regions. The X_R index is defined as the ratio between the intensity of the crystalline fraction and the total intensity of the selected section.

An alternative approach to quantify the crystallinity of the material is to analyze the intensity of the whole diffraction pattern⁴⁰. In this case, the intensity of the whole diffraction pattern, $I_T(Q)$, is determined as a function of the magnitude of the scattering vector $Q = 4\pi\sin(\theta)/\lambda$. The azimuthally averaged intensity of the amorphous halo, $I_A(Q)$, can be calculated by azimuthal integration in selected regions, where it is considered that the intensity arising from Bragg peaks is negligible as shown in Figure 2d. The total intensity of the Bragg peaks is then obtained as: $\Sigma I_B = I_T(Q) - I_A(Q)$. The ratio between the integrated intensity of Bragg peaks and the integrated total intensity defines the $\chi (= \Sigma I_B / I_T)$ index to quantify crystallinity.

Scherrer's equation $L = (0.9\lambda) / (B\cos\theta)$, where B is the radial width (FWHM) of the Gaussian fitted for the diffraction spot, was used to determine the crystallite size⁴¹. L corresponds to a lower size limit for coherently scattering crystallites. Finally, the measure of the orientation of the nanocrystals is obtained from the full width at half maximum (FWHM) of the gaussian used to fit the equatorial peaks (100) in the azimuthal profile obtained from radial integration at the corresponding fixed Bragg angle⁴².

AFM analysis was performed on longitudinal sections of fibers previously embedded in Spurr's resin²¹. The longitudinal sections were obtained by ultramicrotomy with a diamond blade. The AFM images were recorded in a Cervantes AFM system (Nanotec Electrónica, Spain) using Olympus OMCL RC800PSA cantilevers, and the highest resolution was obtained with the stiffest tip (nominal stiffness 0.76 N/m). AFM images were recorded in the dynamic mode in the repulsive regime of the tip-sample interaction⁴³. The processing of the AFM images, consisting of simply equalizing and adjusting the contrast and the brightness of the micrographs, was performed with WSxM program (Nanotec Electrónica, Spain)⁴⁴. No filter was used to improve the quality of the images or to highlight their details.

- Gatesy, J., Hayashi, C., Motriuk, D., Woods, J. & Lewis, R. Extreme diversity, conservation, and convergence of spider silk fibroin sequences. *Science* **291**, 2603–2605 (2001).
- Kaplan, D. L., Lombardi, S., Muller, W. S. & Fossey, S. A. in *Biomaterials. Novel Materials from Biological Sources*. 53 (Stockton Press, New York, 1991).
- Work, R. W. & Emerson, P. D. An Apparatus and Technique for the Forcible Silking of Spiders. *J. Arachnol.* **10**, 1–10 (1982).
- Termonia, Y. Molecular Modeling of Spider Silk Elasticity. *Macromolecules* **27**, 7378–7381 (1994).
- Gosline, J. M., Denny, M. W. & Demont, M. E. Spider Silk as Rubber. *Nature* **309**, 551–552 (1984).
- Termonia, Y. in *Structural Biological Materials* (ed Elices, M.) 335–349 (Pergamon Press, Amsterdam, 2000).
- Work, R. W. Dimensions, Birefringences, and Force-Elongation Behavior of Major and Minor Ampullate Silk Fibers from Orb-Web-Spinning Spiders - Effects of Wetting on these Properties. *Text. Res. J.* **47**, 650–662 (1977).
- Hinman, M. B., Jones, J. A. & Lewis, R. V. Synthetic spider silk: a modular fiber. *Trends Biotechnol.* **18**, 374–379 (2000).
- Vollrath, F. & Edmonds, D. T. Modulation of the Mechanical-Properties of Spider Silk by Coating with Water. *Nature* **340**, 305–307 (1989).
- Blackledge, T. A. & Hayashi, C. Y. Silken toolkits: biomechanics of silk fibers spun by the orb web spider *Argiope argentata* (Fabricius 1775). *J. Exp. Biol.* **209**, 2452–2461 (2006).
- Guinea, G. V., Cerdeira, M., Plaza, G. R., Elices, M. & Perez-Rigueiro, J. Recovery in Viscid Line Fibers. *Biomacromolecules* **11**, 1174–1179 (2010).
- Opell, B. D. & Hendricks, M. L. Adhesive recruitment by the viscous capture threads of araneoid orb-weaving spiders. *J. Exp. Biol.* **210**, 553–560 (2007).
- Guinea, G. V., Elices, M., Perez-Rigueiro, J. & Plaza, G. R. Stretching of supercontracted fibers: a link between spinning and the variability of spider silk. *J. Exp. Biol.* **208**, 25–30 (2005).
- Lefevre, T., Boudreault, S., Cloutier, C. & Pezolet, M. Diversity of Molecular Transformations Involved in the Formation of Spider Silks. *J. Mol. Biol.* **405**, 238–253 (2011).
- Lefevre, T. & Pezolet, M. Unexpected beta-sheets and molecular orientation in flagelliform spider silk as revealed by Raman spectromicroscopy. *Soft Matter* **8**, 6350–6357 (2012).
- Riekkel, C. et al. Aspects of X-ray diffraction on single spider fibers. *Int. J. Biol. Macromol.* **24**, 179–186 (1999).
- Heim, M., Keerl, D. & Scheibel, T. Spider silk: from soluble protein to extraordinary fiber. *Angew. Chem. Int. Ed Engl.* **48**, 3584–96 (2009).
- Riekkel, C. in *Spiderwebs and silk: Tracing evolution from molecules to genes to phenotypes* (ed Craig, C. L.) 51–82 (Oxford University Press, Oxford, 2003).
- Rousseau, M., Lefevre, T. & Pezolet, M. Conformation and Orientation of Proteins in Various Types of Silk Fibers Produced by *Nephila clavipes* Spiders. *Biomacromolecules* **10**, 2945–2953 (2009).
- Plaza, G. R. et al. Relationship between microstructure and mechanical properties in spider silk fibers: two regimes in the microstructural changes. *Soft Matter* **8**, 6015–6026 (2012).
- Perez-Rigueiro, J., Elices, M., Plaza, G. R. & Guinea, G. V. Similarities and differences in the supramolecular organization of silkworm and spider silk. *Macromolecules* **40**, 5360–5365 (2007).
- Nova, A., Keten, S., Pugno, N. M., Redaelli, A. & Buehler, M. J. Molecular and Nanostructural Mechanisms of Deformation, Strength and Toughness of Spider Silk Fibrils. *Nano Letters* **10**, 2626–2634 (2010).
- Tarakanova, A. & Buehler, M. J. A Materiomics Approach to Spider Silk: Protein Molecules to Webs. *JOM* **64**, 214–225 (2012).
- Grubb, D. T. & Jelinski, L. W. Fiber morphology of spider silk: The effects of tensile deformation. *Macromolecules* **30**, 2860–2867 (1997).
- Work, R. W. & Morosoff, N. A. Physicochemical Study of the Supercontraction of Spider Major Ampullate Silk Fibers. *Text. Res. J.* **52**, 349–356 (1982).
- Bratzel, G. & Buehler, M. J. Sequence-structure correlations in silk: Poly-Ala repeat of *N. clavipes* MaSp1 is naturally optimized at a critical length scale. *Journal of the Mechanical Behavior of Biomedical Materials* **7**, 30–40 (2012).
- Keten, S., Xu, Z. P., Ihle, B. & Buehler, M. J. Nanoconfinement controls stiffness, strength and mechanical toughness of beta-sheet crystals in silk. *Nature Materials* **9**, 359–367 (2010).
- Thiel, B. L. & Viney, C. A Nonperiodic Lattice Model for Crystals in *Nephila-Clavipes* Major Ampullate Silk. *MRS Bull* **20** (1995).
- Simmons, A., Michal, C. & Jelinski, L. Molecular orientation and two-component nature of the crystalline fraction of spider dragline silk. *Science* **271**, 84 (1996).



30. Ene, R., Papadopoulos, P. & Kremer, F. Combined structural model of spider dragline silk. *Soft Matter* **5**, 4568–4574 (2009).
31. Paquet-Mercier, F., Lefevre, T., Auger, M. & Pezolet, M. Evidence by infrared spectroscopy of the presence of two types of beta-sheets in major ampullate spider silk and silkworm silk. *Soft Matter* **9**, 208–215 (2013).
32. Li, X., Eles, P. T. & Michal, C. A. Water Permeability of Spider Dragline Silk. *Biomacromolecules* **10**, 1270–1275 (2009).
33. Riekkel, C. & Vollrath, F. Spider silk fibre extrusion: combined wide- and small-angle X-ray microdiffraction experiments. *Int. J. Biol. Macromol.* **29**, 203–210 (2001).
34. Guan, J., Vollrath, F. & Porter, D. Two Mechanisms for Supercontraction in Nephila Spider Dragline Silk. *Biomacromolecules* **12** (2011).
35. Adrianos, S. L. *et al.* Nephila clavipes Flagelliform Silk-Like GGX Motifs Contribute to Extensibility and Spacer Motifs Contribute to Strength in Synthetic Spider Silk Fibers. *Biomacromolecules* **14**, 1751–1760 (2013).
36. Grubb, D. T. & Ji, G. D. Molecular chain orientation in supercontracted and re-extended spider silk. *Int. J. Biol. Macromol.* **24**, 203–210 (1999).
37. Guinea, G. V. *et al.* Minor Ampullate Silks from Nephila and Argiope Spiders: Tensile Properties and Microstructural Characterization. *Biomacromolecules* **13** (2012).
38. Guinea, G. V., Perez-Rigueiro, J., Plaza, G. R. & Elices, M. Volume constancy during stretching of spider silk. *Biomacromolecules* **7**, 2173–2177 (2006).
39. Hammersley, A. FIT2D program, in www.esrf.fr/computing/scientific/FIT2D/ (2009).
40. Martel, A., Burghammer, M., Davies, R. J. & Riekkel, C. Thermal Behavior of Bombyx mori silk: Evolution of crystalline parameters, molecular structure, and mechanical properties. *Biomacromolecules* **8**, 3548–3556 (2007).
41. Klug, H. P. & Alexander, L. in *X-ray Diffraction Procedures for Polycrystalline and Amorphous Materials (2nd ed.)* pp. 618–709. (John Wiley & Sons, New York, USA, 1974).
42. Misra, A., Stein, R. S., Chu, C., Wilkes, G. L. & Desai, A. B. Inducement of Apparent Anisotropic Superstructure in Amorphous Cold Drawn Polyethylene Terephthalate. *Journal of Polymer Science Part C-Polymer Letters* **13**, 303–312 (1975).
43. Garcia, R. & San Paulo, A. Attractive and repulsive tip-sample interaction regimes in tapping-mode atomic force microscopy. *Physical Review B* **60**, 4961–4967 (1999).
44. Horcas, I. *et al.* WSXM: A software for scanning probe microscopy and a tool for nanotechnology. *Rev. Sci. Instrum.* **78** (2007).

Acknowledgements

Spiders were reared in Reptilmadrid S.L. by Oscar Campos. Ultramicrotomy was performed by E. Baldonado (Centro de Microscopía Electrónica, Universidad Complutense de Madrid). Dr. A. Gil and L. Colchero (Nanotec Electrónica, S.L., Spain) offered support for AFM observations. The authors are grateful to José Miguel Martínez for his help with the artwork. The work was funded by Ministerio de Educación y Ciencia (Spain) through project MAT2009-10258, by the Comunidad de Madrid (Spain) (Grant S2011/BMD-2460) and by Fundación Marcelino Botín.

Author contributions

J.P.R. proposed the experiments and wrote the main text. G.B.P. prepared the material and conducted the mechanical tests. C.R. led the XRD analysis, supported by M.B. and R.M. R.D. performed the AFM analysis. G.V.G., C.H., M.E. and G.R.P. contributed to the data analysis and reviewed the manuscript.

Additional information

Competing financial interests: The authors declare no competing financial interests.

How to cite this article: Perea, G.B. *et al.* Identification and dynamics of polyglycine II nanocrystals in *Argiope trifasciata* flagelliform silk. *Sci. Rep.* **3**, 3061; DOI:10.1038/srep03061 (2013).



This work is licensed under a Creative Commons Attribution-NonCommercial-NoDerivs 3.0 Unported license. To view a copy of this license, visit <http://creativecommons.org/licenses/by-nc-nd/3.0>